https://dx.doi.org/10.1016/j.jsv.2015.10.019

Element-by-Element Model Updating of Large-Scale Structures based on Component Mode Synthesis Method

Jie-xin Yu
Fujian Academy of Building Research,
Fujian, China,
Fujian Provincial Key Laboratory of Green Building Technology,
Fujian, China.
e-mail: dark_o@163.com

Yong Xia*
** Corresponding author*
Department of Civil and Environmental Engineering,
The Hong Kong Polytechnic University,
Hong Kong, China
e-mail: ceyxia@polyu.edu.hk

Wei Lin
College of Civil Engineering,
Fuzhou University,
Fujian, China
e-mail: cewlin@fzu.edu.cn

and
Xiao-qing Zhou
College of Civil Engineering,
Shenzhen University,
Guangdong, China
e-mail: xqzhou@szu.edu.cn

Abstract

Component mode synthesis (CMS) method is developed and applied to the element-by-element model updating of large-scale structures in this study. Several lowest frequencies and mode shapes of the global structure are obtained with the free interface CMS method by employing the several lowest frequencies and mode shapes of each substructure individually. In this process, the removal of higher modes is compensated by the residual modes. The eigensensitivity of the global structure is then assembled from the eigensensitivities of each substructure to the updating element parameters. Subsequently, the global model is updated using the sensitivity-based optimization technique. The application of the present method to an 11-floor frame structure and to a large-scale structure demonstrates its accuracy and efficiency. The computational time required by the substructuring method to calculate the eigensensitivity matrices is significantly reduced, as compared with that consumed by the conventional global-based approach. Selection of the number of master modes is also proposed.

Keywords: model updating; substructure method; component mode synthesis; damage detection

I. INTRODUCTION

Structural damage induces changes in physical properties (damping, mass, and stiffness) and accordingly, in the modal properties (frequencies, modal damping, and mode shapes) of the structure. These changes have long been used to identify damage. Model updating technology is an effective approach to solving this inverse problem [1−4]. However, the model updating requires that the global structure needs to be assembled and the eigensolutions and associated eigensensitivity matrices of the global structure need to be calculated repeatedly in each iteration. Consequently the global structure based model updating is very time-consuming and even prohibitive for large-scale structures [5].

The substructuring approach may be employed efficiently in the structural analysis of large-scale structures [6−10]. In this technique, the global structure is divided into small manageable substructures, each of which is analyzed independently to obtain its designated solution. These solutions are then assembled to recover the solutions of the global structure by imposing constraints at the interfaces. Dynamic substructuring methods have been developed in structural dynamics since the 1960s. These methods fall into three categories: the time, frequency, and modal domains [11]. In particular, the modal domain methods use the eigenmodes of each substructure and impose displacement compatibility and force equilibrium conditions on the interfaces between the substructures. This type of technique is commonly referred to as component mode synthesis (CMS). Depending on the interface condition of the substructures, CMS methods can be classified as the free interface [12−14], fixed interface [15, 16], or hybrid method [17, 18]. Numerous such methods have been developed to calculate the eigensolutions [19, 20] of large-scale structures. Recently, the CMS method was developed to obtain the first- and second-order eigensensitivities with respect to modeling uncertainty [21]. Nevertheless, the substructuring method is promising for application in model

updating or damage identification fields. When one or more substructures are modified, the modified substructures alone need to be reanalyzed while others remain unchanged. Liu et al. [22] and Papadimitriou and Papadioti [23] developed the component-based model updating technique, which updates the parameters at the substructure level. However, in practical applications, for example, structural damage detection, one may need to know the damage location and quantity at the element level, rather than the substructure level. In the case, the elemental parameters need to be updated.

An element-by-element model updating technique is proposed in the present paper based on a substructuring approach. The free interface CMS method is developed to calculate eigensolutions and the associated eigensensitivities with respect to element parameters. These values are then applied to the model updating of the global structure. Each substructure is analyzed independently during the updating process. The eigensolutions and eigensensitivities are computed only for particular substructures that contain the updating parameters. Thus, calculation is simplified and accelerated. Two numerical frame examples are used to demonstrate the effectiveness and efficiency of the proposed method. The results show that the proposed method can reduce computation load while maintaining accuracy.

II. FREE INTERFACE COMPONENT MODE SYNTHESIS METHOD

The free interface CMS method developed by Craig and Chang [12] is introduced comprehensively in this section.

For example, a global structure contains N degrees of freedom (DOFs), and its stiffness and mass matrices are of size $N \times N$. For brevity, this structure is divided into two substructures *a* and *b*, with N_a and N_b

DOFs, respectively. When substructure a is taken as an example, the equation of motion in the undamped case is expressed as

$$\mathbf{M}^{(a)}\ddot{\mathbf{x}}^{(a)} + \mathbf{K}^{(a)}\mathbf{x}^{(a)} = \mathbf{f}^{(a)}, \tag{1}$$

where $\mathbf{x}^{(a)}$ and $\ddot{\mathbf{x}}^{(a)}$ are the displacement and acceleration vectors, respectively, with a size of $N_a \times 1$; $\mathbf{M}^{(a)}$ and $\mathbf{K}^{(a)}$ are the mass and stiffness matrices, respectively, with a size of $N_a \times N_a$; and $\mathbf{f}^{(a)}$ is the force vector. Superscript "(a)" denotes the item of substructure a throughout the paper. In the case of free vibration, $\mathbf{f}^{(a)}$ is zero, except for the interface force from the adjacent substructure. The displacement can be written in the modal space as

$$\mathbf{x}^{(a)} = \mathbf{\Phi}^{(a)}\mathbf{p}^{(a)}, \tag{2}$$

where $\mathbf{\Phi}^{(a)}$ represents the eigenvector matrix of the substructure with a size of $N_a \times N_a$, and $\mathbf{p}^{(a)}$ is the modal coordinate.

Eq. (2) can be rewritten according to the lower and higher modes as

$$\mathbf{x}^{(a)} = \begin{bmatrix}\mathbf{\Phi}_l^{(a)} & \mathbf{\Phi}_h^{(a)}\end{bmatrix}\begin{Bmatrix}\mathbf{p}_l^{(a)} \\ \mathbf{p}_h^{(a)}\end{Bmatrix} = \mathbf{\Phi}_l^{(a)}\mathbf{p}_l^{(a)} + \mathbf{\Phi}_h^{(a)}\mathbf{p}_h^{(a)}, \tag{3}$$

where $\mathbf{\Phi}_l^{(a)}$ represents the lower modes with a size of $N_a \times N_{al}$ and $\mathbf{\Phi}_h^{(a)}$ denotes the higher modes with a size of $N_a \times N_{ah}$ ($N_{al} + N_{ah} = N_a$). By substituting Eq. (3) into Eq. (1) and pre-multiplying both sides by $\left(\mathbf{\Phi}^{(a)}\right)^{\mathrm{T}}$, we have

$$\mathbf{I}_l^{(a)}\ddot{\mathbf{p}}_l^{(a)} + \mathbf{\Omega}_l^{(a)}\mathbf{p}_l^{(a)} = \left(\mathbf{\Phi}_l^{(a)}\right)^{\mathrm{T}}\left(\mathbf{B}^{(a)}\right)^{\mathrm{T}}\mathbf{f}_J^{(a)}, \tag{4}$$

$$\mathbf{I}_h^{(a)}\ddot{\mathbf{p}}_h^{(a)} + \mathbf{\Omega}_h^{(a)}\mathbf{p}_h^{(a)} = \left(\mathbf{\Phi}_h^{(a)}\right)^{\mathrm{T}}\left(\mathbf{B}^{(a)}\right)^{\mathrm{T}}\mathbf{f}_J^{(a)}, \tag{5}$$

where $\boldsymbol{\Omega}_l$ and $\boldsymbol{\Omega}_h$ are eigenvalue matrices for the lower and higher modes, respectively; $\mathbf{I}$ is the identity matrix; $\mathbf{B}^{(a)}$ is the Boolean matrix and is described in Appendix; $\mathbf{f}_J^{(a)}$ represents the interface force with a size of $N_J \times 1$; and N_J is the number of interface DOFs.

When the inertia force is much smaller than the restoring force in Eq. (5) (as detailed in subsequent sections), the first item can be neglected. Consequently the modal coordinate associated with the higher modes can be approximated as

$$\mathbf{p}_h^{(a)} = \left(\boldsymbol{\Omega}_h^{(a)}\right)^{-1}\left(\boldsymbol{\Phi}_h^{(a)}\right)^{\mathrm{T}}\left(\mathbf{B}^{(a)}\right)^{\mathrm{T}}\mathbf{f}_J^{(a)}. \tag{6}$$

Eq. (6) is also referred to as the quasi-static response of the high modes. By substituting Eq. (6) into Eq. (3), one has

$$\mathbf{x}^{(a)} = \boldsymbol{\Phi}_l^{(a)}\mathbf{p}_l^{(a)} + \boldsymbol{\psi}_h^{(a)}\mathbf{f}_J^{(a)} = \begin{bmatrix}\boldsymbol{\Phi}_l^{(a)} & \boldsymbol{\psi}_h^{(a)}\end{bmatrix}\begin{Bmatrix}\mathbf{p}_l^{(a)} \\ \mathbf{f}_J^{(a)}\end{Bmatrix}, \tag{7}$$

where

$$\boldsymbol{\psi}_h^{(a)} = \boldsymbol{\Phi}_h^{(a)}\left(\boldsymbol{\Omega}_h^{(a)}\right)^{-1}\left(\boldsymbol{\Phi}_h^{(a)}\right)^{\mathrm{T}}\left(\mathbf{B}^{(a)}\right)^{\mathrm{T}}. \tag{8}$$

Given that the flexibility matrix can be divided into lower and higher modes as

$$\left(\mathbf{K}^{(a)}\right)^{-1} = \boldsymbol{\Phi}^{(a)}\left(\boldsymbol{\Omega}^{(a)}\right)^{-1}\left(\boldsymbol{\Phi}^{(a)}\right)^{\mathrm{T}} = \boldsymbol{\Phi}_l^{(a)}\left(\boldsymbol{\Omega}_l^{(a)}\right)^{-1}\left(\boldsymbol{\Phi}_l^{(a)}\right)^{\mathrm{T}} + \boldsymbol{\Phi}_h^{(a)}\left(\boldsymbol{\Omega}_h^{(a)}\right)^{-1}\left(\boldsymbol{\Phi}_h^{(a)}\right)^{\mathrm{T}}, \tag{9}$$

we define

$$\mathbf{G}^{(a)} = \left(\mathbf{K}^{(a)}\right)^{-1}\left(\mathbf{B}^{(a)}\right)^{\mathrm{T}} = \boldsymbol{\Phi}_l^{(a)}\left(\boldsymbol{\Omega}_l^{(a)}\right)^{-1}\left(\boldsymbol{\Phi}_l^{(a)}\right)^{\mathrm{T}}\left(\mathbf{B}^{(a)}\right)^{\mathrm{T}} + \boldsymbol{\Phi}_h^{(a)}\left(\boldsymbol{\Omega}_h^{(a)}\right)^{-1}\left(\boldsymbol{\Phi}_h^{(a)}\right)^{\mathrm{T}}\left(\mathbf{B}^{(a)}\right)^{\mathrm{T}} = \boldsymbol{\psi}_a^{(a)} + \boldsymbol{\psi}_h^{(a)}, \tag{10}$$

where $\boldsymbol{\psi}_a^{(a)}$ and $\boldsymbol{\psi}_h^{(a)}$ represent the contributions of the lower and higher modes to the flexibility matrix, respectively. $\boldsymbol{\psi}_h^{(a)}$ can be calculated as

$$\boldsymbol{\psi}_h^{(a)} = \mathbf{G}^{(a)} - \boldsymbol{\psi}_a^{(a)}. \tag{11}$$

If a substructure is floating, then the inverse of $\mathbf{K}^{(a)}$ is unavailable. In this case, the rigid-body modes are disregarded. The flexibility matrix with rigid-body modes can then be written as [12, 18]

$$\mathbf{G}^{(a)} = \left(\mathfrak{R}^{(a)}\right)^{\mathrm{T}} \mathbf{G}_c^{(a)} \mathfrak{R}^{(a)} \left(\mathbf{B}^{(a)}\right)^{\mathrm{T}}, \tag{12}$$

where $\mathfrak{R}^{(a)}$ is the projector and is expressed as

$$\mathfrak{R}^{(a)} = \mathbf{I}^{(a)} - \mathbf{M}^{(a)} \boldsymbol{\Phi}_R^{(a)} \left(\boldsymbol{\Phi}_R^{(a)}\right)^{\mathrm{T}}. \tag{13}$$

$\boldsymbol{\Phi}_R^{(a)}$ are the rigid-body modes and $\mathbf{G}_c^{(a)}$ is the flexibility matrix constructed by setting zeros at the constraint DOFs.

The residual flexibility in Eq. (7) serves as one modal base and compensates for the discarded higher modes. The interface force is the corresponding general coordinate. The residual modes improve the accuracy of the substructuring method significantly. By substituting Eq. (7) into Eq. (1) and pre-multiplying both sides by $\left[\boldsymbol{\Phi}_l^{(a)} \quad \boldsymbol{\psi}_h^{(a)}\right]^{\mathrm{T}}$, we have

$$\begin{bmatrix} \mathbf{I}_l^{(a)} & \mathbf{0} \\ \mathbf{0} & \mathbf{M}_G^{(a)} \end{bmatrix} \begin{Bmatrix} \ddot{\mathbf{p}}_l^{(a)} \\ \ddot{\mathbf{f}}_J^{(a)} \end{Bmatrix} + \begin{bmatrix} \boldsymbol{\Omega}_l^{(a)} & \mathbf{0} \\ \mathbf{0} & \mathbf{K}_G^{(a)} \end{bmatrix} \begin{Bmatrix} \mathbf{p}_l^{(a)} \\ \mathbf{f}_J^{(a)} \end{Bmatrix} = \left[\boldsymbol{\Phi}_l^{(a)} \quad \boldsymbol{\psi}_h^{(a)}\right]^{\mathrm{T}} \left(\mathbf{B}^{(a)}\right)^{\mathrm{T}} \mathbf{f}_J^{(a)}, \tag{14}$$

where $\mathbf{M}_G^{(a)}$ and $\mathbf{K}_G^{(a)}$ are the residual mass and residual stiffness matrices, respectively. They are computed as follows

$$\mathbf{M}_G^{(a)} = \left(\boldsymbol{\psi}_h^{(a)}\right)^{\mathrm{T}} \mathbf{M}^{(a)} \boldsymbol{\psi}_h^{(a)}, \ \mathbf{K}_G^{(a)} = \left(\boldsymbol{\psi}_h^{(a)}\right)^{\mathrm{T}} \mathbf{K}^{(a)} \boldsymbol{\psi}_h^{(a)}. \tag{15}$$

Eq. (14) can be rewritten as

$$\widetilde{\mathbf{M}}^{(a)} \ddot{\mathbf{p}}^{(a)} + \widetilde{\mathbf{K}}^{(a)} \mathbf{p}^{(a)} = \left[\boldsymbol{\Phi}_l^{(a)} \quad \boldsymbol{\psi}_h^{(a)}\right]^{\mathrm{T}} \left(\mathbf{B}^{(a)}\right)^{\mathrm{T}} \mathbf{f}_J^{(a)}, \tag{16}$$

where

$$\widetilde{\mathbf{M}}^{(a)}=\begin{bmatrix}\mathbf{I}_l^{(a)} & \mathbf{0}\\ \mathbf{0} & \mathbf{M}_G^{(a)}\end{bmatrix},\ \widetilde{\mathbf{K}}^{(a)}=\begin{bmatrix}\boldsymbol{\Omega}_l^{(a)} & \mathbf{0}\\ \mathbf{0} & \mathbf{K}_G^{(a)}\end{bmatrix},\ \mathbf{p}^{(a)}=\begin{Bmatrix}\mathbf{p}_l^{(a)}\\ \mathbf{f}_J^{(a)}\end{Bmatrix}. \tag{17}$$

The size of the equations presented above is $\left(N_{al}+N_J\right)$. The equation of motion for substructure *b* can be obtained in a similar manner. The two sets of equations are combined as:

$$\begin{bmatrix}\widetilde{\mathbf{M}}^{(a)} & \mathbf{0}\\ \mathbf{0} & \widetilde{\mathbf{M}}^{(b)}\end{bmatrix}\begin{Bmatrix}\ddot{\mathbf{p}}^{(a)}\\ \ddot{\mathbf{p}}^{(b)}\end{Bmatrix}+\begin{bmatrix}\widetilde{\mathbf{K}}^{(a)} & \mathbf{0}\\ \mathbf{0} & \widetilde{\mathbf{K}}^{(b)}\end{bmatrix}\begin{Bmatrix}\mathbf{p}^{(a)}\\ \mathbf{p}^{(b)}\end{Bmatrix}$$

$$=\begin{bmatrix}\left[\boldsymbol{\Phi}_l^{(a)} \quad \boldsymbol{\psi}_h^{(a)}\right]^{\mathrm{T}}\left(\mathbf{B}^{(a)}\right)^{\mathrm{T}} & \mathbf{0}\\ \mathbf{0} & \left[\boldsymbol{\Phi}_l^{(b)} \quad \boldsymbol{\psi}_h^{(b)}\right]^{\mathrm{T}}\left(\mathbf{B}^{(b)}\right)^{\mathrm{T}}\end{bmatrix}\begin{Bmatrix}\mathbf{f}_J^{(a)}\\ \mathbf{f}_J^{(b)}\end{Bmatrix}=\begin{Bmatrix}\mathbf{F}^{(a)}\\ \mathbf{F}^{(b)}\end{Bmatrix}. \tag{18}$$

Similarly superscript "(*b*)" denotes the item of substructure *b*. Substructures *a* and *b* are joined at the common interface. The displacement compatibility and force equilibrium conditions at the interface are expressed by the following equations:

$$\mathbf{x}_J^{(a)}=\mathbf{x}_J^{(b)}. \tag{19}$$

$$\mathbf{f}_J^{(a)}=-\mathbf{f}_J^{(b)}. \tag{20}$$

Given $\mathbf{x}_J^{(a)}=\mathbf{B}^{(a)}\mathbf{x}^{(a)}$ and $\mathbf{x}_J^{(b)}=\mathbf{B}^{(b)}\mathbf{x}^{(b)}$ (see Appendix) and Eq. (7), Eq. (19) can be transformed as

$$\mathbf{B}^{(a)}\left(\boldsymbol{\Phi}_l\mathbf{p}_l+\boldsymbol{\psi}_h\mathbf{f}_J\right)^{(a)}=\mathbf{B}^{(b)}\left(\boldsymbol{\Phi}_l\mathbf{p}_l+\boldsymbol{\psi}_h\mathbf{f}_J\right)^{(b)}. \tag{21}$$

Combining Eqs. (20) and (21), the interface force can be solved as

$$\mathbf{f}_J^{(a)}=-\mathbf{f}_J^{(b)}=\left[\left(\mathbf{B}\boldsymbol{\psi}_h\right)^{(a)}+\left(\mathbf{B}\boldsymbol{\psi}_h\right)^{(b)}\right]^{-1}\left[\left(\mathbf{B}\boldsymbol{\Phi}_l\mathbf{p}_l\right)^{(b)}-\left(\mathbf{B}\boldsymbol{\Phi}_l\mathbf{p}_l\right)^{(a)}\right]. \tag{22}$$

Thus, the modal coordinates of the two substructures can be transformed into those associated with the lower modes:

$$\mathbf{p}=\begin{Bmatrix}\mathbf{p}^{(a)}\\ \mathbf{p}^{(b)}\end{Bmatrix}=\begin{Bmatrix}\mathbf{p}_l^{(a)}\\ \mathbf{f}_J^{(a)}\\ \mathbf{p}_l^{(b)}\\ \mathbf{f}_J^{(b)}\end{Bmatrix}=\begin{bmatrix}\mathbf{I} & \mathbf{0}\\ \mathbf{A} & \mathbf{D}\\ \mathbf{0} & \mathbf{I}\\ -\mathbf{A} & -\mathbf{D}\end{bmatrix}\begin{Bmatrix}\mathbf{p}_l^{(a)}\\ \mathbf{p}_l^{(b)}\end{Bmatrix}=\mathbf{T}\mathbf{q}, \tag{23}$$

where

$$\mathbf{A} = -\left[\left(\mathbf{B}\boldsymbol{\psi}_h\right)^{(a)} + \left(\mathbf{B}\boldsymbol{\psi}_h\right)^{(b)}\right]^{-1}\left(\mathbf{B}\boldsymbol{\Phi}_l\right)^{(a)},$$

$$\mathbf{D} = \left[\left(\mathbf{B}\boldsymbol{\psi}_h\right)^{(a)} + \left(\mathbf{B}\boldsymbol{\psi}_h\right)^{(b)}\right]^{-1}\left(\mathbf{B}\boldsymbol{\Phi}_l\right)^{(b)}. \tag{24}$$

$\mathbf{q}$ is the modal coordinate associated with the lower modes of the two substructures and has a size of $\left(N_{al} + N_{bl}\right)\times 1$. $\mathbf{T}$ is the transformation matrix with a size of $\left(N_{al} + N_{bl} + 2N_J\right)\times\left(N_{al} + N_{bl}\right)$.

By substituting Eq. (23) into Eq. (18) and pre-multiplying both sides by $\mathbf{T}^{\mathrm{T}}$, we have

$$\mathbf{M}^*\ddot{\mathbf{q}} + \mathbf{K}^*\mathbf{q} = \mathbf{0}, \tag{25}$$

where

$$\mathbf{M}^* = \mathbf{T}^{\mathrm{T}}\widetilde{\mathbf{M}}\mathbf{T},\ \mathbf{K}^* = \mathbf{T}^{\mathrm{T}}\widetilde{\mathbf{K}}\mathbf{T}. \tag{26}$$

The right-hand side of Eq. (25) is calculated as zero because the forces at the interface always appear in pairs. Eq. (25) is the final standard eigenequation of the assembled global structure with a size of $\left(N_{al} + N_{bl}\right)$. Assuming that its eigensolutions are $\boldsymbol{\Omega}^*$ and $\boldsymbol{\Phi}^*$, the eigenvalues of the original system are $\boldsymbol{\Omega}^*$ and the eigenvectors are transformed as

$$\boldsymbol{\Phi} = \begin{bmatrix} \boldsymbol{\Phi}^{(a)} & \\ & \boldsymbol{\Phi}^{(b)} \end{bmatrix}\mathbf{T}\boldsymbol{\Phi}^* = \boldsymbol{\Phi}^p\mathbf{T}\boldsymbol{\Phi}^*, \tag{27}$$

where superscript '*p*' denotes the diagonal assembly of the substructural matrices. As only a few lower modes of each substructure are included, the size of the reduced eigenequation $\left(N_{al} + N_{bl}\right)$ is much smaller than the global one (N). As a result, solving the large eigenequation is avoided. Nevertheless, the eigensolution is less computationally difficult to solve at present than before given the rapid development of computer technology. The main advantage of the substructuring method lies in the calculation of the eigensensitivity value. This process is more time-consuming than the computation of eigensolutions and is frequently required in iterative model updating.

III. ELEMENT-BY-ELEMENT SENSITIVITY-BASED MODEL UPDATING METHOD

Structural damages may cause changes in structural responses. Model updating aims to reproduce the true (or experimental) dynamic properties of a structure by iteratively adjusting the parameters of the structural model optimally. The sensitivity-based model updating method is a widely employed approach [5, 24].

In this approach, experimental responses can be expressed as the first order Taylor expansion of the structural element parameters in the form of the following equation:

$$\mathbf{R}_e - \mathbf{R}_o = \mathbf{S}(\mathbf{r}_u - \mathbf{r}_o). \tag{28}$$

where $\mathbf{R}_e$ and $\mathbf{R}_o$ represent the experimental and analytical responses of the structure, respectively; $\mathbf{r}_u$ and $\mathbf{r}_o$ are the corresponding structural parameter vectors; and $\mathbf{S}$ is the sensitivity matrix (or eigensensitivity when modal data are used) that can be obtained by taking derivatives of the responses with respect to the structural parameters. Without losing generality, each element has one parameter for updating in this study.

During the optimization process, the elemental parameters in the analytical model are iteratively modified to match the experimental vibration properties. The eigensolutions and the eigensensitivity matrix of the analytical model must be calculated in each iteration [24]. Traditional model updating methods calculate these values based on the system matrices of the global structure. This procedure is time-consuming and computationally expensive, especially when the structure is composed of a large number of DOFs.

In the present study, the substructuring method is applied to obtain the sensitivity matrix. According to Eq. (25), the eigenequation of the ith mode (i =1, 2, …, N) can be written as

$$\left(\mathbf{K}^* - \mathbf{M}^*\lambda_i\right)\mathbf{\Phi}_i^* = \mathbf{0}. \tag{29}$$

Eq. (29) is differentiated with respect to parameter r as follows:

$$\frac{\partial\left(\mathbf{K}^* - \mathbf{M}^*\lambda_i\right)}{\partial r}\mathbf{\Phi}_i^* + \left(\mathbf{K}^* - \mathbf{M}^*\lambda_i\right)\frac{\partial\mathbf{\Phi}_i^*}{\partial r} = \mathbf{0}. \tag{30}$$

Pre-multiplying $\left(\mathbf{\Phi}_i^*\right)^{\mathrm{T}}$ both sides of Eq. (30) yields the following equation:

$$\left(\mathbf{\Phi}_i^*\right)^{\mathrm{T}}\frac{\partial\left(\mathbf{K}^* - \mathbf{M}^*\lambda_i\right)}{\partial r}\mathbf{\Phi}_i^* + \left(\mathbf{\Phi}_i^*\right)^{\mathrm{T}}\left(\mathbf{K}^* - \mathbf{M}^*\lambda_i\right)\frac{\partial\mathbf{\Phi}_i^*}{\partial r} = \mathbf{0}. \tag{31}$$

$\left(\mathbf{K}^* - \mathbf{M}^*\lambda_i\right)$ is symmetric and $\left(\mathbf{K}^* - \mathbf{M}^*\lambda_i\right)\mathbf{\Phi}_i^* = \mathbf{0}$. Therefore, Eq. (31) can be simplified as

$$\left(\mathbf{\Phi}_i^*\right)^{\mathrm{T}}\frac{\partial\left(\mathbf{K}^* - \mathbf{M}^*\lambda_i\right)}{\partial r}\mathbf{\Phi}_i^* = \mathbf{0}. \tag{32}$$

Given the normalization property of $\mathbf{\Phi}_i^*$, the derivative of eigenvalue λ_i can be obtained as

$$\frac{\partial\lambda_i}{\partial r} = \left(\mathbf{\Phi}_i^*\right)^{\mathrm{T}}\frac{\partial\mathbf{K}^*}{\partial r}\mathbf{\Phi}_i^*. \tag{33}$$

For simplicity, $\partial\mathbf{K}^*/\partial r$ is calculated with the finite difference technique.

The ith eigenvector of the global structure can be recovered by

$$\mathbf{\Phi}_i = \mathbf{\Phi}^p\mathbf{T}\mathbf{\Phi}_i^*. \tag{34}$$

The eigenvector derivative of the ith mode to structural parameter r is differentiated as

$$\frac{\partial\mathbf{\Phi}_i}{\partial r} = \frac{\partial\mathbf{\Phi}^p}{\partial r}\mathbf{T}\mathbf{\Phi}_i^* + \mathbf{\Phi}^p\mathbf{T}\frac{\partial\mathbf{\Phi}_i^*}{\partial r}. \tag{35}$$

$\mathbf{T}$, $\mathbf{\Phi}^p$, and $\mathbf{\Phi}_i^*$ are obtained in the process of calculating the eigensolutions. $\partial\mathbf{\Phi}^p/\partial r$ is the eigenvector derivative of the substructure containing parameter r and thus can be calculated within the substructure.

$\partial\boldsymbol{\Phi}^*/\partial r$ can be calculated using Nelson's method [25]; that is, it consists of a particular part and a homogeneous part as

$$\frac{\partial\boldsymbol{\Phi}_i^*}{\partial r}=\mathbf{v}_i+c_i\boldsymbol{\Phi}_i^*, \tag{36}$$

where c_i is the participation factor. By substituting Eq. (36) into Eq. (30), we have the following equation:

$$\left(\mathbf{K}^*-\mathbf{M}^*\lambda_i\right)\left(\mathbf{v}_i+c_i\boldsymbol{\Phi}_i^*\right)=-\frac{\partial\left(\mathbf{K}^*-\mathbf{M}^*\lambda_i\right)}{\partial r}\boldsymbol{\Phi}_i^*. \tag{37}$$

Given that $\left(\mathbf{K}^*-\mathbf{M}^*\lambda_i\right)\boldsymbol{\Phi}_i^*=\mathbf{0}$, Eq. (37) can be simplified as

$$\mathbf{X}_i\mathbf{v}_i=\mathbf{Y}_i, \tag{38}$$

where

$$\mathbf{X}_i=\left(\mathbf{K}^*-\mathbf{M}^*\lambda_i\right),\ \mathbf{Y}_i=-\frac{\partial\left(\mathbf{K}^*-\mathbf{M}^*\lambda_i\right)}{\partial r}\boldsymbol{\Phi}_i^*. \tag{39}$$

$\partial\mathbf{K}^*/\partial r$ has been calculated in Eq. (33). $\partial\mathbf{M}^*/\partial r=0$ because the mass presumably remains unchanged during model updating. Consequently, vector $\mathbf{v}_i$ can be solved using Eq. (38).

The solution of c_i requires the orthogonal condition of the eigenvector

$$\left(\boldsymbol{\Phi}_i^*\right)^{\mathrm{T}}\mathbf{M}^*\boldsymbol{\Phi}_i^*=1. \tag{40}$$

Differentiating Eq. (40) with respect to *r* produces

$$\frac{\partial\left(\boldsymbol{\Phi}_i^*\right)^{\mathrm{T}}}{\partial r}\mathbf{M}^*\boldsymbol{\Phi}_i^*+\left(\boldsymbol{\Phi}_i^*\right)^{\mathrm{T}}\frac{\partial\mathbf{M}^*}{\partial r}\boldsymbol{\Phi}_i^*+\left(\boldsymbol{\Phi}_i^*\right)^{\mathrm{T}}\mathbf{M}^*\frac{\partial\boldsymbol{\Phi}_i^*}{\partial r}=\mathbf{0}. \tag{41}$$

Given $\partial\mathbf{M}^*/\partial r=0$, Eq. (41) is simplified into

$$\frac{\partial\left(\boldsymbol{\Phi}_i^*\right)^{\mathrm{T}}}{\partial r}\mathbf{M}^*\boldsymbol{\Phi}_i^*+\left(\boldsymbol{\Phi}_i^*\right)^{\mathrm{T}}\mathbf{M}^*\frac{\partial\boldsymbol{\Phi}_i^*}{\partial r}=\mathbf{0}. \tag{42}$$

By substituting Eq. (36) into Eq. (42), we obtain

$$\left[\left(\mathbf{v}_i\right)^{\mathrm{T}} + c_i\left(\boldsymbol{\Phi}_i^*\right)^{\mathrm{T}}\right]\mathbf{M}\boldsymbol{\Phi}_i^* + \left(\boldsymbol{\Phi}_i^*\right)^{\mathrm{T}}\mathbf{M}^*\left(\mathbf{v}_i + c_i\boldsymbol{\Phi}_i^*\right) = \mathbf{0}. \tag{43}$$

Participation factor c_i is thus obtained as

$$c_i = -\frac{1}{2}\left(\left(\mathbf{v}_i\right)^{\mathrm{T}}\mathbf{M}^*\boldsymbol{\Phi}_i^* + \left(\boldsymbol{\Phi}_i^*\right)^{\mathrm{T}}\mathbf{M}^*\mathbf{v}_i\right). \tag{44}$$

Subsequently, the first-order derivative of $\boldsymbol{\Phi}_i^*$ with respect to structural parameter *r* is obtained as

$$\frac{\partial\boldsymbol{\Phi}_i^*}{\partial r} = \mathbf{v}_i - \frac{1}{2}\left[\left(\mathbf{v}_i\right)^{\mathrm{T}}\mathbf{M}^*\boldsymbol{\Phi}_i^* + \left(\boldsymbol{\Phi}_i^*\right)^{\mathrm{T}}\mathbf{M}^*\mathbf{v}_i\right]. \tag{45}$$

IV. NUMERICAL EXAMPLES

Two numerical examples are employed to demonstrate the effectiveness and efficiency of the proposed substructuring model updating method. The accuracy of CMS method is first validated by calculating the eigensolutions and eigensensitivities of two structures. CMS-based model updating is then applied to identify damage. The results obtained with this method are compared with those generated using the traditional model updating approach.

1. CMS-based eigensolution

As shown in Fig. 1, the 11-floor frame structure considered in this study consists of a total of 79 nodes, 88 two-dimensional elements, and 231 DOFs. The frame is disassembled into three substructures that contain 30, 30, and 23 nodes, as well as 84, 90, and 69 DOFs. These substructures are depicted in Fig. 1(b). Each substructure is analyzed independently to calculate its eigensolutions and eigensensitivities. These values are then assembled into the global ones using the proposed method.

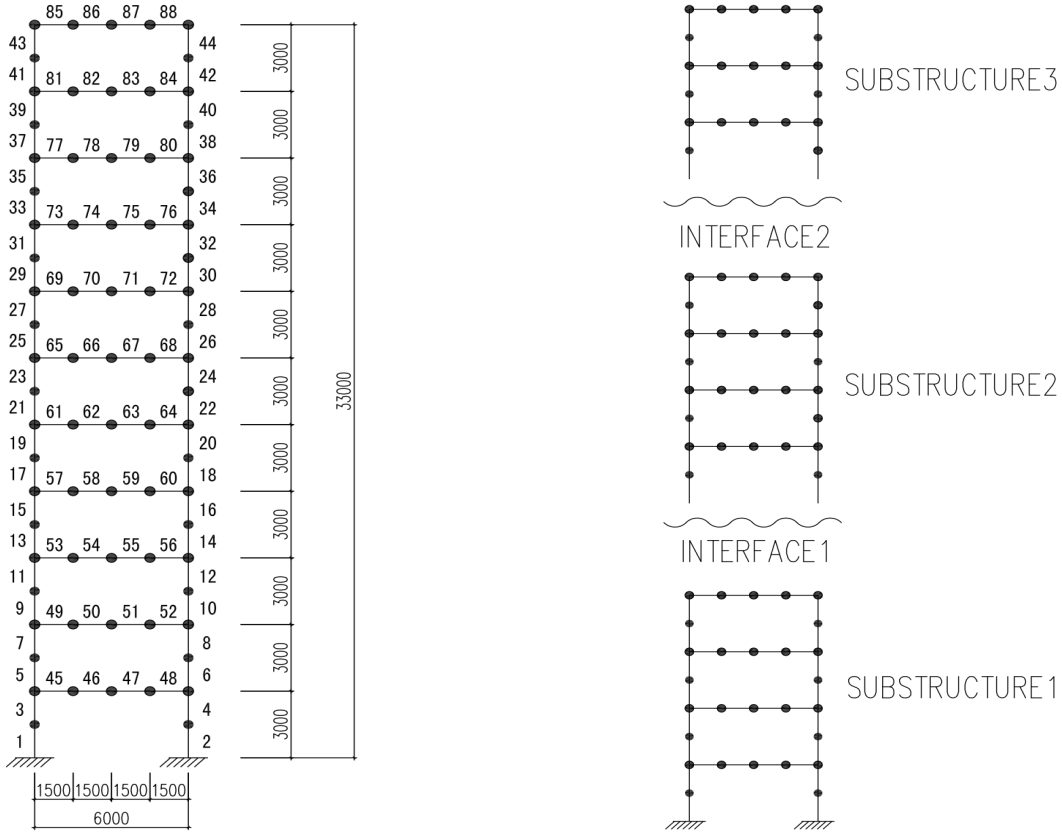

(a) Global structure (b) Partitioned substructures

Fig. 1. Frame structure (unit: m)

A criterion of modal truncation is proposed to select the master modes of each substructure. According to Eq. (5), the first item (inertia force) should be much smaller than the second (restoring force). For example, the subsystem vibrates at frequency ω and amplitude b, that is, $p_h = b\sin(\omega t)$ and $\ddot{p}_h = -\omega^2 b\sin(\omega t)$. Thus, the following formulas are generated

$$\left|\omega^2 b\sin(\omega t)\right| << \left|\omega_h{}^2 b\sin(\omega t)\right|. \tag{46}$$

$$\lambda << \lambda_h . \tag{47}$$

This scenario indicates that the discarded eigenvalues of the substructure must be significantly larger than the eigenvalues of interest associated with the global structure. In this study, we set

$$\lambda_h > 100\lambda . \tag{48}$$

This equation implies that the largest eigenvalue retained in the substructure must be 100 times the largest eigenvalue of interest associated with the global structure.

In this example, we assume that the first 10 modes are of interest. The 10^{th} eigenvalue of the global structure is 47,625 rad^2/s^2. The first 38 modes of each substructure are listed in Table 1. According to the criteria, the first 33, 36, and 28 modes of the three substructures are retained and assembled to calculate the first 10 modes of the global structure. The discarded higher modes are compensated by the residual flexibility modes, as discussed in section II. The calculated frequencies are listed and compared with the true values using the traditional method in Table 2. The similarity of the two sets of mode shapes is listed as well in terms of the modal assurance criterion (MAC) [26].

Table 1. Eigenvalues of Substructures

Mode	Eigenvalue			Mode	Eigenvalue			Mode	Eigenvalue		
	Sub 1	Sub 2	Sub 3		Sub 1	Sub 2	Sub 3		Sub 1	Sub 2	Sub 3
1	810.96	0	0	14	6.49E+5	4.60E+5	7.53E+5	27	2.60E+6	2.20E+6	4.45E+6
2	9170.8	0	0	15	7.16E+5	4.96E+5	7.66E+5	28	2.79E+6	2.24E+6	5.60E+6
3	34603	0	0	16	7.94E+5	6.50E+5	1.01E+6	29	2.93E+6	2.45E+6	6.81E+6
4	48501	7828.3	9808.8	17	8.54E+5	7.17E+5	1.17E+6	30	3.50E+6	2.79E+6	7.10E+6
5	60738	13772	19977	18	1.06E+6	7.61E+5	1.29E+6	31	3.86E+6	2.93E+6	7.95E+6
6	67385	19932	26073	19	1.14E+6	7.81E+5	1.43E+6	32	4.63E+6	3.24E+6	8.40E+6
7	75999	41212	54493	20	1.35E+6	7.97E+5	1.74E+6	33	4.84E+6	3.41E+6	9.87E+6
8	82095	53590	76828	21	1.48E+6	1.01E+6	2.13E+6	34	6.04E+6	3.63E+6	1.08E+7
9	1.51E+5	68354	77502	22	1.68E+6	1.05E+6	2.23E+6	35	7.02E+6	4.33E+6	1.12E+7
10	2.57E+5	79227	1.28E+5	23	2.08E+6	1.17E+6	2.49E+6	36	7.43E+6	4.77E+6	1.27E+7
11	3.82E+5	87505	3.97E+5	24	2.09E+6	1.36E+6	2.79E+6	37	7.65E+6	6.57E+6	1.27E+7
12	4.89E+5	1.30E+5	4.98E+5	25	2.23E+6	1.77E+6	3.19E+6	38	8.17E+6	7.11E+6	1.44E+7
13	5.46E+5	3.76E+5	6.61E+5	26	2.44E+6	2.04E+6	3.49E+6	⋮	⋮	⋮	⋮

Table 2. Frequency and MAC of the Assembled Global Structure

Mode No.	Frequency			MAC (%)
	Traditional method (Hz)	Substructuring method (Hz)	Relative error (%)	
1	1.448	1.448	0.0	100.0
2	4.537	4.539	0.0	100.0
3	8.233	8.234	0.0	100.0
4	12.300	12.301	0.0	100.0
5	17.011	17.016	0.0	100.0
6	18.855	18.971	0.6	100.0
7	22.286	22.294	0.0	100.0
8	26.256	26.390	0.5	100.0
9	28.417	28.416	0.0	100.0
10	34.732	34.733	0.0	100.0

Table 2 shows that the relative errors of the first 10 frequencies are less than 0.6%, and the MAC values are all 100.0%. These values are sufficiently accurate for model updating. This example verifies the effectiveness of the free interface CMS method. In addition, the proposed criterion of modal truncation can significantly reduce the number of modes retained in each substructure while maintaining high accuracy.

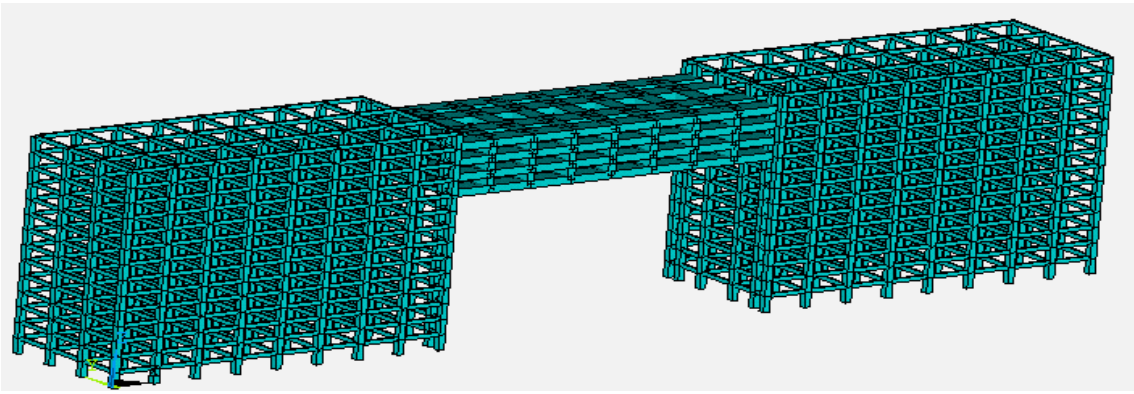

Fig. 2. Large-scale frame structure

The proposed method is also applied to a practical large-scale structure to study its computational efficiency. This structure is displayed in Fig. 2 and consists of two symmetric towers that are linked by one corridor. Each tower has 14 floors, with a total height of 45 m. The corridor is located at an elevation of 29 m and has three floors. It is 19.8 m wide and 67.2 m high. The finite element (FE) model contains a total of 1,252 nodes, 3,190 elements, and 7,512 DOFs. Overall, the traditional global approach takes 864.2 s to calculate the first 10 modes using a personal computer with a Core 2 Duo CPU and 2 GB memory. The proposed CMS method is thus utilized to reduce computational load.

First, the global structure is divided into five substructures, as illustrated in Fig. 3. The retained modes are selected according to the proposed criterion of modal truncation. The detailed information regarding the substructures is listed in Table 3.

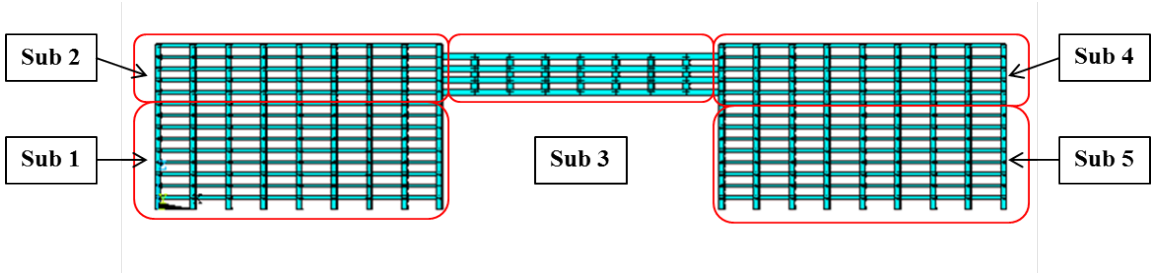

Fig. 3. Configuration of division scheme 1

Table 3. Division Formation Scheme 1

Substructure index	Sub 1	Sub 2	Sub 3	Sub 4	Sub 5
No. of nodes	304	304	144	304	304
No. of DOFs	1596	1824	864	1824	1596
No. of elements	693	693	296	693	693
No. of interface nodes	38	54	32	54	38
No. of retained modes	82	146	14	146	82

Another two division schemes, that is, schemes 2 and 3, are also employed to determine the influence of the substructure division on calculation accuracy and efficiency. Division schemes 2 and 3 consist of nine and three substructures, respectively, as indicated in Figs. 4 and 5. The substructure information for these two division schemes is listed in Tables 4 and 5.

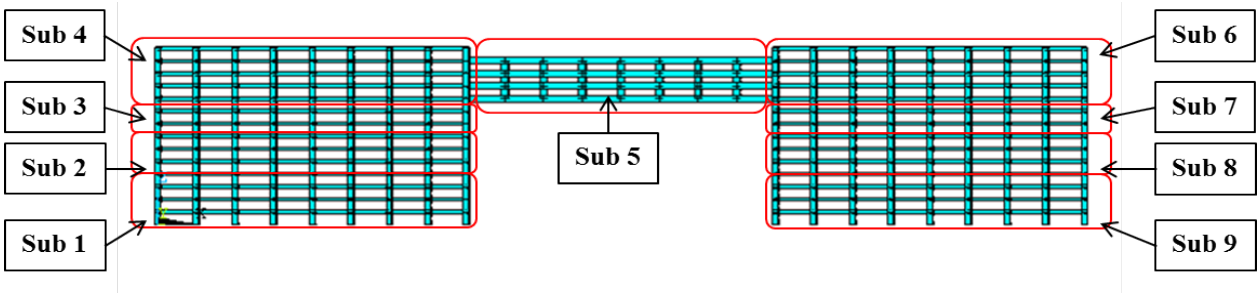

Fig. 4. Configuration of division scheme 2

Table 4. Division Formation Scheme 2

Substructure index	Sub 1	Sub 2	Sub 3	Sub 4	Sub 5	Sub 6	Sub 7	Sub 8	Sub 9
No. of nodes	190	152	114	228	144	228	144	152	190
No. of DOFs	912	912	684	1368	864	1368	684	912	912
No. of elements	364	273	182	455	296	455	182	273	364
No. of interface nodes	38	76	76	54	32	54	76	76	38
No. of retained modes	46	103	94	123	14	123	94	103	46

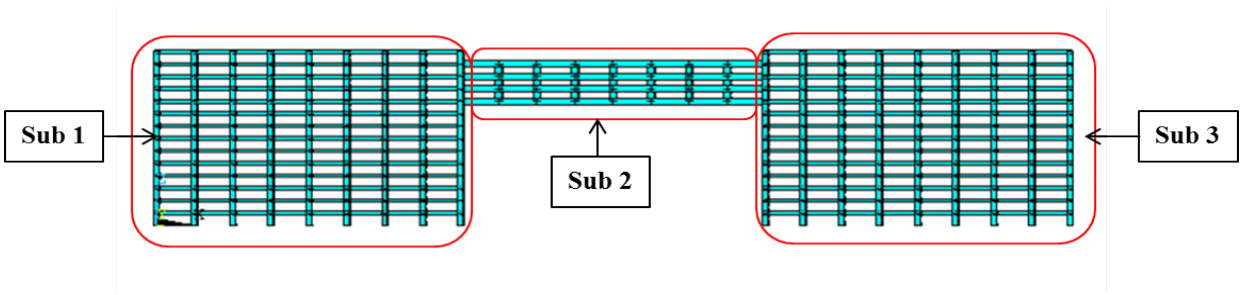

Fig. 5. Configuration of division scheme 3

Table 5. Division Formation Scheme 3

Substructure index	Sub 1	Sub 2	Sub 3
No. of nodes	570	144	570
No. of DOFs	3420	864	3420
No. of elements	1447	296	1447
No. of interface nodes	16	32	16
No. of retained modes	170	14	170

The first 10 eigensolutions of the global structure are calculated in all division schemes. The results are compared in Table 6, in which the true results are calculated using the global method. All three division formations are precise.

Table 6. Comparison of the Eigensolutions of Each Division Scheme

Mode	True freq. (Hz)	Scheme 1			Scheme 2			Scheme 3		
		Freq. (Hz)	Relative error (%)	MAC (%)	Freq. (Hz)	Relative error (%)	MAC (%)	Freq. (Hz)	Relative error (%)	MAC (%)
1	0.584	0.585	0.1	100.0	0.586	−0.3	100.0	0.585	0.1	100.0
2	0.744	0.746	0.2	100.0	0.740	0.6	100.0	0.744	0.0	100.0
3	0.873	0.875	0.2	99.9	0.873	0.1	99.0	0.873	0.0	100.0
4	0.895	0.895	0.0	100.0	0.89	0.5	100.0	0.895	0.0	100.0
5	0.939	0.943	0.3	99.8	0.946	−0.7	98.0	0.939	0.0	100.0
6	1.025	1.025	0.0	100.0	1.021	0.4	100.0	1.025	0.0	100.0
7	1.038	1.039	0.1	100.0	1.038	0.0	99.4	1.038	0.0	100.0
8	1.237	1.237	0.0	100.0	1.234	0.3	100.0	1.237	0.0	100.0
9	1.266	1.267	0.0	100.0	1.265	0.1	99.9	1.266	0.0	100.0
10	1.544	1.544	0.0	100.0	1.542	0.2	100.0	1.544	0.0	100.0

358 Table 7. Comparison of the Times Consumed in Each Division Scheme

Division scheme	Scheme 1	Scheme 2	Scheme 3	Global method
Size of the assembled structure	470	746	354	7512
Number of substructures	5	9	3	-
CPU time (s)	227.2	289.4	652.8	864.2

359

360 The CPU time costs in the three division formations and in the global method are compared in Table 7.
361 Scheme 3, which includes three substructures, consumes the most computational time. By contrast, scheme
362 1, which contains five substructures, consumes the least time. When a structure is divided into a large
363 number of substructures, each substructure contains a small number of DOFs whereas the number of
364 interfaces increases. Consequently, the assembled eigenequation is large, as indicated in scheme 2. By
365 contrast, if a structure is divided into a small number of substructures, then each substructure still has a large
366 number of DOFs. Correspondingly, the process of calculating the eigensolutions and the residual flexibility
367 matrix of each substructure is heavy. This example shows that dividing the global structure into either
368 excessive or insufficient substructures is inefficient. Five substructures result in the ideal computational
369 efficiency in the present example. It is noted that the optimal division scheme is structurally dependent, and
370 no conclusions are drawn for general structures. Trial and error can be performed before model updating.

371

372 *2. CMS-based eigensensitivity*

373

374 The 11-floor frame structure shown in Fig. 1 is utilized in this study to determine the accuracy of the
375 proposed CMS method in calculating eigensensitivity. The eigenvalue and eigenvector derivatives for the
376 first 10 modes of the global structure with respect to element 1 are listed in Table 8. These values are
377 compared with those obtained using the traditional global method. The relative differences of all eigenvalue

derivatives are less than 3.5%, and the similarity values of all eigenvector derivatives are above 99.8%. These percentages indicate sufficient accuracy for model updating.

Table 8. Comparison of Eigensensitivity with respect to Element 1

Mode No.	Eigenvalue derivative			MAC of eigenvector derivative (%)
	Traditional method	Substructuring method	Relative error (%)	
1	9.2443×10^{-11}	9.2490×10^{-11}	0.1	100.0
2	8.2750×10^{-10}	8.2871×10^{-10}	0.1	100.0
3	2.5883×10^{-9}	2.5879×10^{-9}	0.0	100.0
4	5.7376×10^{-9}	5.7423×10^{-9}	0.1	100.0
5	1.0599×10^{-8}	1.0611×10^{-8}	0.1	100.0
6	1.6242×10^{-8}	1.6599×10^{-8}	2.2	99.8
7	1.7506×10^{-8}	1.7499×10^{-8}	0.0	100.0
8	2.6518×10^{-8}	2.7435×10^{-8}	3.5	99.9
9	2.5773×10^{-8}	2.5830×10^{-8}	0.2	100.0
10	3.3993×10^{-8}	3.3986×10^{-8}	0.0	100.0

3. CMS-based model updating

The proposed method is then applied to the first structure for model updating and damage detection. Damage is simulated by reducing the bending rigidity of chosen elements. The modal data in the damaged state are calculated on the basis of the damaged FE model. Subsequently, the analytical model is updated using the proposed substructuring method such that the modal data of the updated model match those of the damaged ones. The changes in the bending rigidity of each element are treated as identified damage, and this damage is compared with the actual ones. Three simulated damage scenarios are listed in Table 9. The first 10 frequencies and modes are utilized during model updating. The mode shapes are determined at the horizontal direction of the nodes on columns and at the vertical direction of the middle nodes on beams. As

393 before, the first 33, 36, and 28 modes in substructures 1, 2, and 3 are chosen as the master modes to calculate
394 the first 10 eigensolutions and eigensensitivities of the global structure. The higher modes are compensated
395 by the residual flexibility modes.

396 Table 9. Simulated Damage Scenarios

Case	Damaged element	Reduction of bending rigidity
1	No. 61	−40%
2	Nos. 7 and 57	−40%, −30%
3	Nos. 10, 17, and 77	−10%, −20%, −30%

397

398 In the first case, the bending rigidity of element 61 (located in the second substructure) is presumably
399 reduced by 40% while the other elements remain unchanged. The identified damage results obtained using
400 the traditional global method and those using the proposed method are compared in Fig. 6. Both methods
401 can detect damage location and severity successfully. The computational times consumed by the
402 substructuring and the global methods are 478.8 and 837.2 s, respectively. Therefore, the proposed
403 substructuring method is more efficient than the global method in terms of damage detection.

404

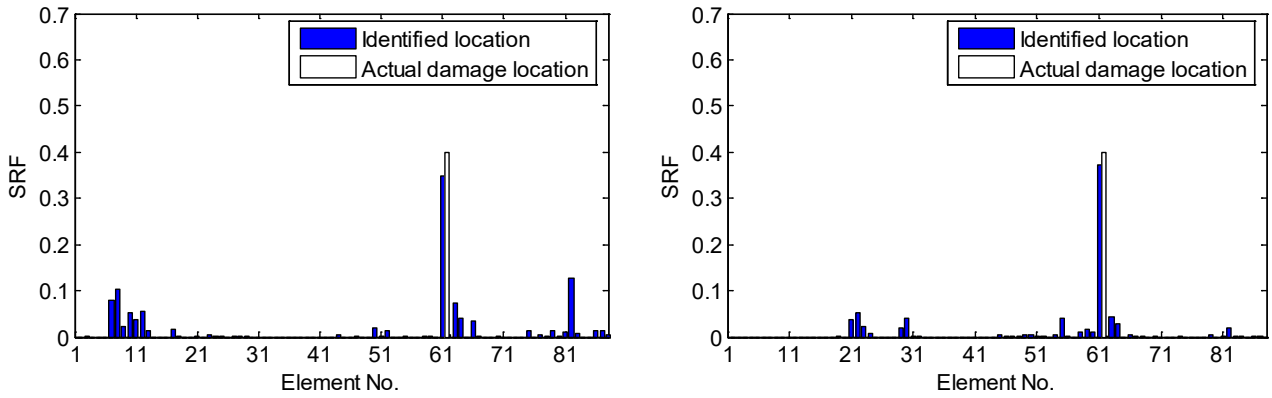

(a) Substructuring method (b) Global method

Fig. 6. Location and severity of identified damage (Case 1)

In the second case, one column element and one beam element in the first substructure are simulated as damaged. That is, the bending rigidities of elements 7 and 57 are presumably reduced by 40% and 30%, respectively. Model updating is performed using both methods, and the damage identification results are compared in Fig. 7. Similarly, both approaches can detect damage successfully. The total times consumed by the substructuring and the global methods are 316.25 and 610.53 s, respectively. Therefore, the proposed method is more efficient than the traditional global one.

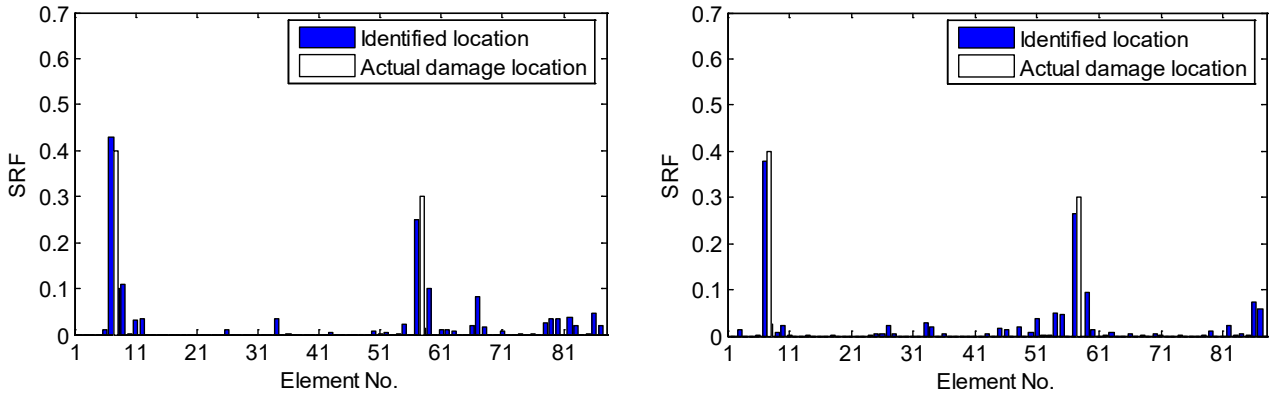

(a) Substructuring method (b) Global method

Fig. 7. Location and severity of identified damage (Case 2)

The third case involves damage to different substructures. In particular, the bending rigidities of element 10 in substructure 1, element 17 in substructure 2, and element 77 in substructure 3 are presumably reduced by 10%, 20%, and 30%, respectively. This aims to test the damage identifiability of the technique. The damage detection results are illustrated in Fig. 8. Both methods can successfully detect the damaged elements with 20% and 30% stiffness reduction, whereas have errors in detecting the slightest damage with 10% stiffness reduction. The computational times consumed by the substructuring and the global methods are 301.5 and

580.34 s, respectively. Once again, the proposed substructuring method is more computationally efficient than the global method is.

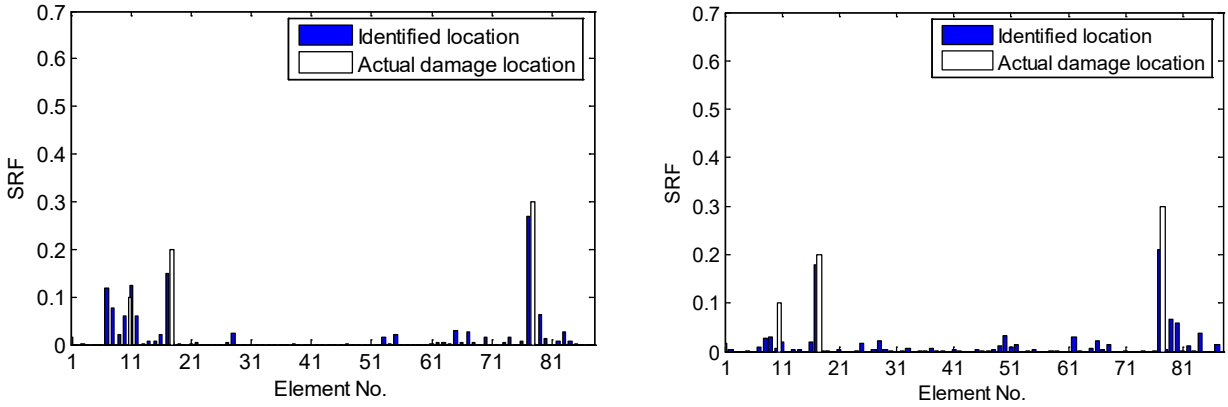

(a) Substructuring method (b) Global method

Fig. 8. Location and severity of identified damage (Case 3)

The three damage identification events verify that the location and severity of the assumed reduction in elemental stiffness can be identified successfully with the proposed substructure-based model updating method except for the minor damage case. This proposed method displays a higher computational efficiency in terms of damage detection than the traditional global method does.

V. CONCLUSIONS

CMS-based substructuring method is developed in this study for model updating at the element level. The method divides the global structure into several manageable substructures and calculates the eigensolutions and eigensensitivities of each substructure with respect to the element parameters independently. Lower master modes of each substructure are retained according to a proposed mode truncation criterion, and residual modal flexibility is used to compensate for the discarded higher modes. The substructural results

436 are then assembled to obtain the global counterparts for iterative model updating. The method is applied to
437 an 11-floor frame structure, and the numerical example shows that simulated damage can be detected
438 accurately using the substructuring method except for the minor damage case. Furthermore, this method
439 requires less computational effort than traditional global model updating does.
440
441 A large-scale structure with over seven thousand DOFs is also used to calculate the eigensolutions with
442 different substructuring division schemes. The division formation must trade off the number of
443 substructures and the master modes in each substructure. An excessive or insufficient number of
444 substructures may increase computational load.
445
446 Numerical examples also show that minor damage in structural members may not be detected accurately
447 because it causes a small change in the vibration properties. In addition, measurement noise and modeling
448 errors may mask this small change and cause the identification results deviate from the real ones. Sensitivity
449 of the proposed method merits further study.
450
451
452 ## ACKNOWLEDGMENT
453
454 This research is supported by the National Natural Science Foundation of China (Project No. 51328802) and
455 the RISUD of The Hong Kong Polytechnic University (Project No. 4-ZZCF).
456
457

458

459 APPENDIX

460

461 Let $\mathbf{x}^{(a)}$ be the $N_a \times 1$ displacement vector of substructure *a* and $\mathbf{x}_J^{(a)}$ the $N_J \times 1$ displacement vector of the

462 interface between adjacent substructures. Their relation is represented by the following equation:

463 $$\mathbf{x}_J^{(a)} = \mathbf{B}^{(a)}\mathbf{x}^{(a)}, \tag{A.1}$$

464 where $\mathbf{B}^{(a)}$ is the Boolean matrix with a size of $N_J \times N_a$. Each row of matrix $\mathbf{B}^{(a)}$ contains only one

465 non-zero item, which takes a value of 1 at the corresponding interface DOF. Let $\mathbf{f}^{(a)}$ be the force vector of

466 the substructure. Given a free vibration case, $\mathbf{f}^{(a)}$ is zero except at the interface. Let $\mathbf{f}_J^{(a)}$ be the interface

467 force with a size of $N_J \times 1$. Then, we obtain

468 $$\mathbf{f}^{(a)} = \left(\mathbf{B}^{(a)}\right)^{\mathrm{T}} \mathbf{f}_J^{(a)}. \tag{A.2}$$

469 Therefore, the Boolean matrix links the displacement and the force between the substructure and the global

470 structure.

471

472

473

474 REFERENCES

475

476 [1] C. P. Fritzen, D. Jennewein, T. Kiefer, Damage detection based on model updating methods,
477 *Mechanical Systems and Signal Processing* 12 (1998) 163-186.
478 [2] A. Teughels, G. De Roeck, Structural damage identification of the highway bridge Z24 by FE model
479 updating, *Journal of Sound and Vibration* 278 (2004) 589-610.
480 [3] W. X. Ren, Z. S. Sun, Y. Xia, H. Hao, A. J. Deeks, Vibration-based damage identification of shear
481 connectors in bridge decks: laboratory test study, *Journal of Structural Engineering* 134 (2008)
482 832-841.
483 [4] O.S. Salawu, Detection of structural damage through changes in frequency: a review, *Engineering*
484 *Structures* 19 (1997) 718–723.
485 [5] Y. Xia, H. Hao, A. J. Deeks, Dynamic assessment of shear connectors in slab-girder bridges,
486 *Engineering Structures* 29 (2007) 1475-1486.
487 [6] C.G. Koh, B. Hong, C.Y. Liaw, Substructural and progressive structural identification methods,
488 *Engineering Structures* 25 (2003) 1551–1563.
489 [7] J. Li, S.S. Law, Y. Ding, Substructure damage identification based on response reconstruction in
490 frequency domain and model updating, *Engineering Structures* 41 (2007) 270-284.
491 [8] R.R. Craig, S.E.M. Sem, A brief tutorial on substructure analysis and testing, *The 18th IMAC*
492 *Conference on Computational Challenges in Structural Dynamics*, San Antonio, TX, 2000, pp.
493 899-908.
494 [9] M. Lou, A. Ghobarah, T.S. Aziz, Application of Wilson-Ritz vectors in dynamic substructuring,
495 *International Journal of Solids and Structures* 30 (1993) 3159-3170.
496 [10] D. Choi, H. Kim, M. Cho, Iterative method for dynamic condensation combined with substructuring
497 scheme, *Journal of Sound and Vibration* 317 (2008) 199-218.
498 [11] D. de Klerk, D. J. Rixen, S. N. Voormeeren, General framework for dynamic substructuring: history,
499 review, and classification of techniques, *AIAA Journal* 46 (2008) 1169-1181.
500 [12] R. R. Craig, C. J. Chang, Free-interface methods of substructure coupling for dynamic analysis,
501 *AIAA Journal* 14 (1976) 1633-1635.
502 [13] S. Rubin, Improved component-mode representation for structural dynamic analysis, *AIAA Journal*
503 13 (1975) 995-1006.

504 [14] D. J. Rixen, A dual Craig–Bampton method for dynamic substructuring, *Journal of Computational*
505 *and Applied Mathematics* 168 (2004) 383–391.
506 [15] W. C. Hurty, Dynamic analysis of structural systems using component modes, *AIAA Journal* 3 (1965)
507 678-685.
508 [16] R. R. Craig, Jr, M. C. C. Bampton, Coupling of substructures for dynamic analyses, *AIAA Journal* 6
509 (1968) 1313-1319.
510 [17] J. Qiu, F. W. Williams, R. Qiu, A new exact substructure method using mixed modes, *Journal of*
511 *Sound and Vibration* 266 (2003) 737–757.
512 [18] R. H. MacNeal, A hybrid method of component mode synthesis, *Computers and Structures* 1 (1971)
513 581–601.
514 [19] S. Weng, Y. Xia, Y.L. Xu, X.Q. Zhou, H.P. Zhu, Improved substructuring method for eigensolutions
515 of large-scale structures, *Journal of Sound and Vibration* 323 (2009) 718-736.
516 [20] S. Weng, Y. Xia, Y.L. Xu, H.P. Zhu, An iterative substructuring approach to the calculation of
517 eigensolution and eigensensitivity, *Journal of Sound and Vibration*, 330 (2011) 3368-3380.
518 [21] Sarsri, D., Azrar, L., Dynamic analysis of large structures with uncertain parameters based on
519 coupling component mode synthesis and perturbation method, *Ain Shams Engineering Journal*
520 Available online 24 April 2015, doi:10.1016/j.asej.2015.03.005.
521 [22] Liu, Y., Sun, H., Wang, D., Updating the finite element model of large-scaled structures using
522 component mode synthesis technique, *Intelligent Automation and Soft Computing* 19 (2013) 11-21.
523 [23] Papadimitriou, C., Papadioti, D.C., Component mode synthesis techniques for finite element model
524 updating, *Computers and Structures* 126 (2013) 15-28.
525 [24] P. G. Bakir, E. Reynders, G. De Roeck, Sensitivity-based finite element model updating using
526 constrained optimization with a trust region algorithm, *Journal of Sound and Vibration* 305 (2007)
527 211-25.
528 [25] Nelson, R. B., Simplified calculation of eigenvector derivatives, *AIAA Journal* 14 (1976)
529 1201–1205.
530 [26] Maia, N.M.M., Silva, J.M.M., He, J., Lieven, N.A.J., Lin, R.M., Skingle, G.W., To, W., Urgueira,
531 A.P.V., *Theoretical and Experimental Modal Analysis*, Research Studies Press Ltd., 1997.
532